

Citation for published version:

Banai, RE, Burton, LA, Choi, SG, Hofherr, F, Sorgenfrei, T, Walsh, A, To, B, Cröll, A & Brownson, JRS 2014, 'Ellipsometric characterization and density-functional theory analysis of anisotropic optical properties of single-crystal -SnS', *Journal of Applied Physics*, vol. 116, no. 1, pp. 013511. <https://doi.org/10.1063/1.4886915>

DOI:

[10.1063/1.4886915](https://doi.org/10.1063/1.4886915)

Publication date:

2014

Document Version

Early version, also known as pre-print

[Link to publication](#)

Publisher Rights

Unspecified

University of Bath

Alternative formats

If you require this document in an alternative format, please contact:
openaccess@bath.ac.uk

General rights

Copyright and moral rights for the publications made accessible in the public portal are retained by the authors and/or other copyright owners and it is a condition of accessing publications that users recognise and abide by the legal requirements associated with these rights.

Take down policy

If you believe that this document breaches copyright please contact us providing details, and we will remove access to the work immediately and investigate your claim.

Ellipsometric characterization and density-functional theory analysis of anisotropic optical properties of single-crystal α -SnS

R.E. Banai,¹ L.A. Burton,² S.G. Choi,^{3,a)} F. Hofherr,⁴ T. Sorgenfrei,⁴ A. Walsh,² B. To,³ A. Cröll,⁴ J.R.S. Brownson¹

¹Department of Materials Science and Engineering, Pennsylvania State University, University Park, Pennsylvania 16802, United States of America

²Centre for Sustainable Chemical Technologies and Department of Chemistry, University of Bath, Claverton Down, Bath BA2 7AY, United Kingdom

³National Renewable Energy Laboratory, Golden, Colorado 80401, United States of America

⁴Crystallography – Institute of Earth and Environmental Sciences, University of Freiburg, 79104 Freiburg, Germany

ABSTRACT

We report on the anisotropic optical properties of single-crystal tin monosulfide (SnS). The components $\bar{E} \parallel \bar{a}$, $\bar{E} \parallel \bar{b}$, and $\bar{E} \parallel \bar{c}$ of the pseudo-dielectric-function tensor $\langle \epsilon \rangle = \langle \epsilon_i \rangle + i\langle \epsilon_i \rangle$ spectra are taken from 0.73 to 6.45 eV by spectroscopic ellipsometry. The measured $\langle \epsilon \rangle$ spectra are in a good agreement with the results of the calculated dielectric response from hybrid density functional theory. The $\langle \epsilon \rangle$ spectra show the direct band-gap onset and a total of eight above-band-gap optical structures that are associated with the interband-transition critical points (CPs). We obtain accurate CP energies by fitting analytic CP expressions to second-energy-derivatives of the $\langle \epsilon \rangle$ data. Their probable electronic origins and implications for photovoltaic applications are discussed.

^aAuthor to whom correspondence should be addressed. Electronic mail: sukgeun.choi@nrel.gov.

I. INTRODUCTION

A natural *p*-type IV-VI binary compound tin monosulfide (SnS) is considered a promising absorber material for the next-generation thin-film photovoltaic (PV) technology. SnS has a suitable band-gap energy of ~ 1.1 eV,¹ a large optical absorption coefficient of 10^4 - 10^5 cm⁻¹ above the band gap,^{2,3} a high intrinsic free carrier concentration of $\sim 10^{17}$ cm⁻³,⁴ and earth abundance of the constituent elements. These properties suggest that PV devices with efficiencies as high as 24% are possible.⁵

Despite material properties that are almost ideal for PV device applications, the power conversion efficiency (η) of SnS solar cells is so far limited to 4.4%,⁶ which is substantially smaller than the values achieved with alternate materials with similar opto-electronic properties.⁷ In attempts to increase the η of SnS solar cells, crystalline quality has been improved,⁸ optimum device architecture has been suggested,⁹ and detrimental effects of the possible secondary phases, such as SnS₂ and Sn₃S₄, on the device performance have been examined.¹⁰

Knowledge of optical properties of materials plays an important role in the development of high-efficiency solar cells.¹¹⁻¹³ Complex refractive index $N = n + ik$ and relevant properties, such as normal-incidence reflectivity R and absorption coefficient α , are used to characterize the device performance.^{14,15} The complex dielectric function $\epsilon = \epsilon_1 + i\epsilon_2$ provides great insight into the electronic structure of materials and can be used to compare experimental data to theoretical predictions,¹⁶⁻¹⁹ which in turn further enhances the performance and functionality of solar cells through *bandgap*- and *defect-engineering*.

For SnS, however, clear discrepancies exist among the reported optical data of polycrystalline thin films.^{3,20-30} In addition, optical properties of reference single-crystal SnS have not been well established, yet. The layer-structured SnS crystallizes in the orthorhombic structure (space group *Pnma*) with the lattice parameters of $a = 4.33$ Å, $b = 3.98$ Å, and $c = 11.18$ Å,³¹ which is depicted in Fig. 1. Therefore, SnS is expected to exhibit anisotropy in its optical

properties. The anisotropic ϵ_s (ϵ at $\vec{E} \parallel \vec{a}$) and ϵ_v (ϵ at $\vec{E} \parallel \vec{b}$) spectra have been derived from a combined analysis of optical transmission and electron-energy-loss spectra from 0.5 to 22 eV.³² The N for a single-crystal SnS, determined by unpolarized transmission measurements,³³ also showed anisotropy in $\vec{E} \parallel \vec{a}$ and $\vec{E} \parallel \vec{b}$. However, details of the optical structures shown in ϵ_s and ϵ_v spectra have not been discussed and the experimental spectrum for ϵ_c (ϵ at $\vec{E} \parallel \vec{c}$) is still not yet available in the literature.

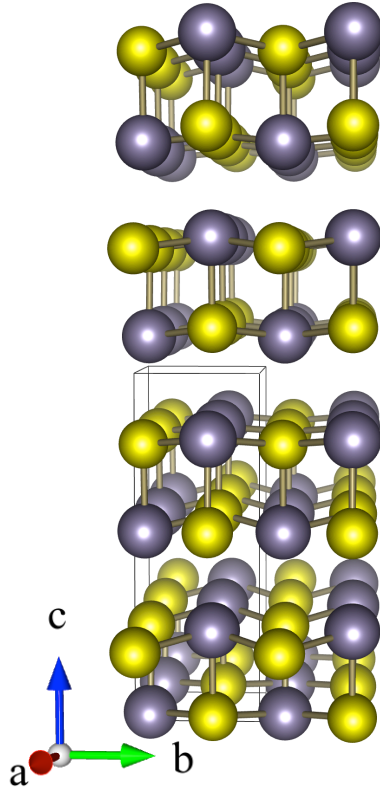


FIG. 1. (Color online) The distorted-rocksalt orthorhombic ($Pnma$) crystal structure of SnS. The Sn atoms are colored dark grey.

Here, we apply spectroscopic ellipsometry (SE) to determine the room-temperature pseudodielectric function $\langle \epsilon_s \rangle$, $\langle \epsilon_v \rangle$, and $\langle \epsilon_c \rangle$ spectra for single-crystal SnS. The SE data show a good agreement with the ϵ_s , ϵ_v , and ϵ_c data calculated by hybrid density functional theory (DFT). In addition to the band-gap onset, a total of eight optical structures associated with the interband-transition critical points (CPs) are shown in the ϵ spectra, and the CP energy values are accurately obtained from the standard line-shape analysis^{34,35} of the numerically calculated

$d\epsilon/dE^2$ data. Electronic origins of CP energies and implications for PV device applications are discussed.

II. EXPERIMENTS

A single crystal SnS bulk was grown by the Bridgman-Stockbarger technique in a sealed fused silica glass ampoule. As starting material, poly-crystal of an *ab-initio* synthesis in a stoichiometric composition was used. For the bulk growth, a vertical resistance furnace consisting of three independent heating zones was used. Before growth, the material was homogenized for 1 hr. in zone 1 at 930°C, which is above the melting point of 880°C. During the growth, the temperature gradient (ΔT) was 13°/cm and the growth rate was 0.5 mm/hr. Details of the growth and structural characterization are given in Ref. [36](#).

For SE measurements, a 2 mm-thick slab was cut from the bulk crystal with a large surface (approximately 100 mm²) normal to the *c* direction. The large surface consisting of *a* and *b* axes and one side-face containing *b* and *c* axes were chemo-mechanically polished to reduce the surface overlayer artifacts. Diamond lapping films with various grit sizes ranging from 30 to 0.1 μm were used in an Allied High Tech Multi Purpose polishing system to progressively polish the surface, and the procedure was completed in conjunction with a 0.05- μm colloidal silica suspension applied on a polishing cloth.

SE measurements were performed in the spectral range of 0.73 to 6.45 eV with the sample maintained at room temperature using a spectroscopic rotating compensator-type ellipsometer (J.A. Woollam Inc., M2000-DI model). The angle of incidence was 70°. The contribution from the ϵ tensor component along the axis normal to the measurement surface is known to be negligible to the SE data, which is reduced approximately by $1/\epsilon$.³⁷ On the other hand, the SE measurement is most sensitive to the ϵ tensor component aligned to the intersecting line drawn by sample surface and plain of incidence.^{37,38} For the SnS crystal used in this study, the *c*-axis is normal to the measurement surface, while the *a* and *b* axes are

embedded within the surface. Hence, the ϵ_i and ϵ_s spectra were acquired by rotating the sample about the surface normal, such that the intersecting line is parallel to the a - and b -axis, respectively, as depicted in Fig. 2(a). Similarly, the ϵ_c spectrum was obtained by taking SE data on a side face of the SnS crystal with the c axis parallel to the intersecting line (Fig. 2(b)).

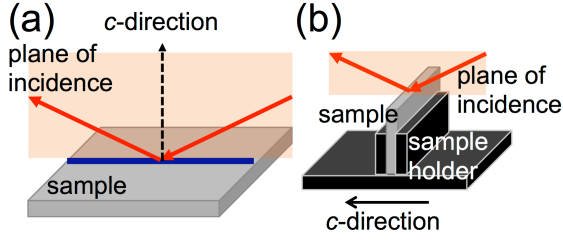


FIG. 2. (Color online) Schematics depicting the SE measurements of (a) the large measurement surface containing the a and b axes, and (b) the polished side-face containing the c axis. A plane of incidence is indicated as the shaded area. For the SE measurement of the side-face, a homemade spring-loaded sample holder was used.

III. COMPUTATIONAL DETAILS

The electronic structure of SnS was calculated within Density Functional Theory (DFT) using a non-local hybrid exchange-correlation functional developed by Heyd, Scuseria, and Ernzerhof (HSE06).³⁹ All calculations were performed using the Vienna Ab-initio Simulation Package (VASP) code,⁴⁰ with the projector augmented wave (PAW) approach,⁴¹ a 400 eV plane wave cut-off, and reciprocal space sampling of $6 \times 6 \times 4$ k -points. The calculations included 240 bands, 40 of which were occupied. Electronic densities of states were calculated using the tetrahedron method with Blöchl corrections.

The structural parameters of SnS were fixed at the experimentally determined room-temperature values of Ref. 42 in order to avoid errors associated with temperature and van der Waals interactions, which are not negligible in this pseudo-layered structure.

The $\epsilon(\omega)$ was calculated within the electric dipole approximation from the real and imaginary hybrid Kohn-Sham eigenstates.⁴² The imaginary part of the frequency dependent dielectric response is computed by:

$$\epsilon_2(\omega) = 1 + \frac{4\pi^2 e^2}{\Omega} \lim_{q \rightarrow 0} \frac{1}{q^2} \sum_{c,v,k} 2\omega_k \delta(\epsilon_{ck} - \epsilon_{vk} - \omega) \times \langle u_{ck+c_\alpha q} | u_{vk} \rangle \langle u_{ck+c_\beta q} | u_{vk} \rangle \quad (1)$$

where c and v refer to the conduction and valence band states respectively, and u_{ck} is the cell periodic part of the orbitals at the k -point k . ω is the frequency of the incident photon and Ω is the volume of the unit cell. The real part of the dielectric tensor is obtained using the standard Kramers-Kronig transformation:

$$\epsilon_1(\omega) = 1 + \frac{2}{\pi} P \int_0^\infty \frac{\epsilon_r^{(2)}(\omega')\omega'}{\omega'^2 - \omega^2 + i\eta} d\omega' \quad (2)$$

where P denotes the principal value and η is the complex shift.

IV. RESULTS AND DISCUSSION

The calculated electronic band structure of SnS is shown in Fig. 3. With the HSE06 treatment of electron exchange and correlation, SnS exhibits a fundamental electronic band gap of 1.11 eV that is spatially indirect, and a direct gap of 1.22 eV. Although the SE data do not resolve it due to low transition intensities, the prediction of indirect gap at 1.11 eV is consistent with the results from other theoretical^{28,44} and experimental^{20,45} studies.

The electronic band dispersion of SnS is typical of a layered material with a relatively flat band structure associated with the weakly interacting layers (longer Sn – S interatomic separation) and more dispersive pattern in the strongly bonded plane. Quadratic fitting to the values of the energy dispersion around the direct band gap between Γ and Y points, shown in Fig. 3, yield effective masses of $0.07m_e$ for holes and $0.12m_e$ for electrons in the b direction. Experimentally observed effective masses for holes along the a and b crystallographic orientations are of the order of $0.2 m_e$ at 300 K determined from free carrier reflectivity.⁴⁶ These values are somewhat larger than those we calculate, which is unsurprising due to the exclusion of temperature and the assumption of a perfect uniform crystal in the model electronic structure.

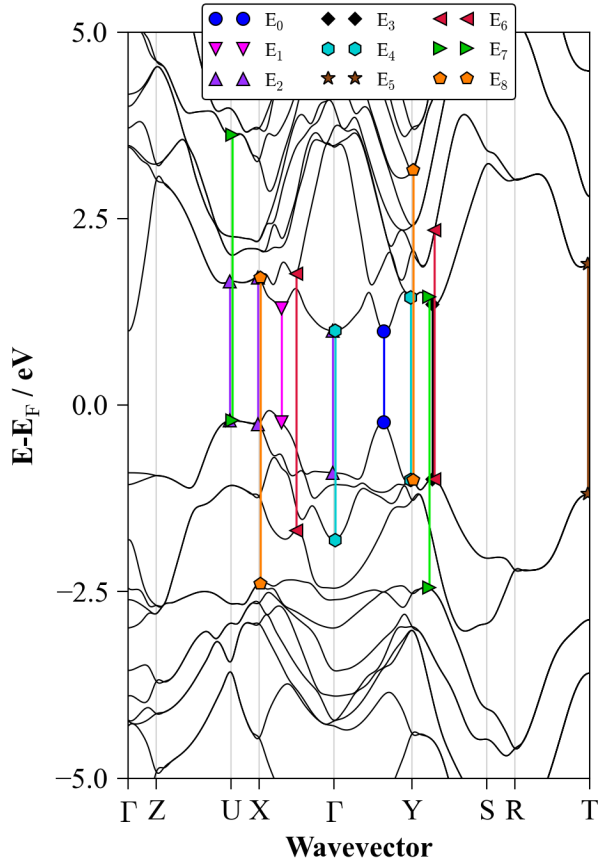


FIG. 3. (Color online) The calculated electronic energy band structure of SnS. The major critical points are identified at various symmetric points of Brillouin zone.

Calculated and SE-determined ϵ_r , ϵ_i , and ϵ spectra are presented in Figs. 4(a – f), showing a good agreement in the overall shape. The calculated dielectric constants for the light polarization $\vec{E} \parallel \vec{a}$, $\vec{E} \parallel \vec{b}$, and $\vec{E} \parallel \vec{c}$ are listed in Table I. The calculated optical dielectric constants ϵ_r are in a good agreement with the SE-determined $\langle \epsilon_r \rangle$ values at the low energy limit: 12.82 for $\vec{E} \parallel \vec{a}$, 15.97 for $\vec{E} \parallel \vec{b}$, and 13.25 for $\vec{E} \parallel \vec{c}$. We note that the SE data shown in Figs. 4(b), (d), and (f) are *pseudodielectric function* $\langle \epsilon \rangle = \langle \epsilon_r \rangle + i\langle \epsilon_i \rangle$ spectra that are the direct inversion of experimental data, where no mathematical data modeling is involved. Nonzero $\langle \epsilon_i \rangle$ value below ~ 1.3 eV can be thus a result of indirect band-gap nature of SnS crystal, a possible presence of thin surface overlayers such as native oxides and microscopic roughness,

or a combination of the preceding. Owing to the uncertainty in the origin of below-band-gap absorption, we did not attempt a multilayer analysis in this study and report the $\langle \epsilon \rangle$ spectra, taken after careful surface preparation procedures, that should be a close approximation to material's intrinsic ϵ data.

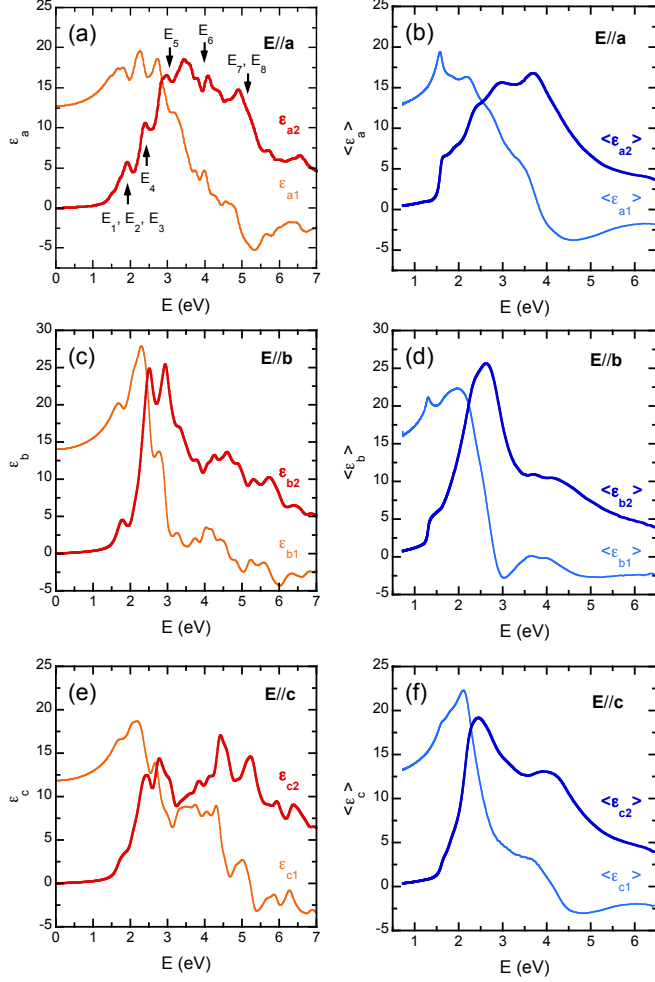


FIG. 4. (Color online) Calculated and SE-determined ϵ spectra for the light polarization $\vec{E} \parallel \vec{a}$ (a,b), $\vec{E} \parallel \vec{b}$ (c,d), and $\vec{E} \parallel \vec{c}$ (e,f). Calculated data are presented in the left column (a,c, and e) and SE-determined $\langle \epsilon \rangle$ spectra are shown in the right column (b,d, and f), respectively. Real part (ϵ_r) and imaginary part (ϵ_i) are shown as light-thin and dark-thick lines, respectively.

The SE-determined $\langle \epsilon \rangle$ spectra for the light polarization $\vec{E} \parallel \vec{a}$ and $\vec{E} \parallel \vec{b}$ are in a good agreement with the data obtained from a combined analysis of optical transmission and electron-energy-loss spectra.³² The ϵ_{a2} spectra (Figs. 4(a) and 4(b)) show one broad optical structure with several fine features spanning from ~ 1.3 to ~ 5.0 eV. As an example, the major

above-band-gap CP structures are identified based on the results of calculated electronic energy band structure (Fig. 3) in Fig. 4(a).

Table I. Calculated high frequency (ϵ_∞) and static (ϵ_0) dielectric constants of SnS (from HSE06-DFT). The ionic contribution to the response is calculated using the phonon dispersion from density functional perturbation theory.

Property	$\vec{E} \parallel \vec{a}$	$\vec{E} \parallel \vec{b}$	$\vec{E} \parallel \vec{c}$
ϵ_{ionic}	21.36	37.64	22.72
ϵ_∞	12.70	14.02	11.85
$\epsilon_0 = \epsilon_\infty + \epsilon_{\text{ionic}}$	34.06	51.66	34.57

In conjunction with the assigned probable vertical transitions (Fig. 3), we can elucidate the origin of the observed optical transitions. The ϵ_{b2} spectra (Figs. 4(c) and 4(d)) can be characterized by a large optical structure at ~ 2.5 eV followed by a weak broad structure centered at ~ 4 eV. The electronic origin of the main peak at ~ 2.5 eV can be identified as a transition primarily from S p and Sn s orbitals in the valence band to Sn p orbitals in the conduction band occurring between the Γ and Y points in the BZ. The high density of transitions within this narrow region of the BZ at similar energies accounts for the comparatively stronger absorption profile in the b direction. For the ϵ_a spectra (Figs. 4(e) and 4(f)), two distinct structures are seen at ~ 2.5 and ~ 4 eV whose electronic origins are understood to be the same as those observed in the ϵ_{b2} spectra. No experimental ϵ spectrum for the light polarization $\vec{E} \parallel \vec{c}$ of SnS is available in the literature to compare with our ϵ_a data, but the calculations reported by Makinistian and Albanesi¹⁸ show similar results.

The direct band-gap energy is one of the key optical parameters of materials for the applications in PV devices. Our SE-determined $\langle \epsilon_\infty \rangle$ spectrum (Fig. 4(d)) shows that the major optical absorption starts at ~ 1.3 eV, whereas the absorption onset in $\langle \epsilon_{a2} \rangle$ and $\langle \epsilon_{a1} \rangle$ spectra (Figs.

4(b) and (f)) seems to appear at slightly higher energy (~1.5 eV), which is consistent with some of the previously reported studies. Makinistian *et al.*⁴⁸ predicted maxima in the dielectric functions of 1.54 eV for the ϵ_{xx} and ϵ_{yy} , and 1.21 eV for the ϵ_{zz} (from semi-local DFT using a scissors operator). A room-temperature electro-reflectance study⁴⁹ also showed that the lowest direct gaps for the polarization of light $\vec{E} \parallel \vec{a}$ and $\vec{E} \parallel \vec{b}$ are 1.6 and 1.3 eV, respectively. Our calculations confirm that SnS has a fundamental direct band gap at 1.22 eV regardless of the light polarization, as discussed earlier, but variation in optical transition intensity introduces the anisotropic response. This behavior will be important for photovoltaic applications in terms of deciding preferential material orientation and morphology, and in optical modeling for optimal device configurations.

In order to verify the theoretical prediction of the band gap at 1.22 eV, we perform the standard lineshape analysis^{44,35} of the SE data, where the $\langle \epsilon \rangle$ spectra are differentiated and smoothed numerically using algorithms of the Savitzky-Golay type,⁵⁰ followed by least-squares fitting of standard analytic CP expressions. The CP expressions are:^{51,52}

$$\frac{d^2 \epsilon}{dE^2} = \begin{cases} n(n-1)Ae^{i\phi}(E - E_g + i\Gamma)^{n-2}, & n \neq 0 \\ Ae^{i\phi}(E - E_g + i\Gamma)^{-2}, & n = 0 \end{cases} \quad (3)$$

where A is the amplitude, E_g is the threshold energy, Γ is the broadening parameter, and ϕ is the phase. The exponent n has values of -1, -1/2, 0, and 1/2 for excitonic, one-, two- and three-dimensional lineshapes, respectively. Real and imaginary parts are fit simultaneously.

Figures 5(a - c) show the $d\langle \epsilon \rangle / dE^2$ spectra (open symbols) together with the best-fit curves (lines) for the polarization of light $\vec{E} \parallel \vec{a}$, $\vec{E} \parallel \vec{b}$, and $\vec{E} \parallel \vec{c}$, respectively. A combination of two- ($n = 0$) and three-dimensional ($n = 1/2$) lineshapes is used to fit the data from 1.0 to 5.0 eV, which results in the minimum discrepancy between the data and fits. Energies of each CP

structure are indicated by arrows and labeled in a numeric order. Differentiation substantially enhances the sensitivity to the weak optical structures, and multiple CP structures are now clearly seen. Even though presence of the optical transition at ~ 1.3 eV is not obvious in the $\langle \epsilon_a \rangle$ and $\langle \epsilon_c \rangle$ spectra shown in Figs. 4(b) and 4(f), it appears in the $d\langle \epsilon_a \rangle/dE^2$ and $d\langle \epsilon_c \rangle/dE^2$ spectra as a small shoulder. Inclusion of this transition in the lineshape analysis improved the quality of fits in the low-energy region of spectra. Unlike the case for $d\langle \epsilon_a \rangle/dE^2$ and $d\langle \epsilon_c \rangle/dE^2$ spectra, the $d\langle \epsilon_b \rangle/dE^2$ spectrum shows a distinct optical structure at ~ 1.3 eV, which is indeed expected from Fig. 4(d).

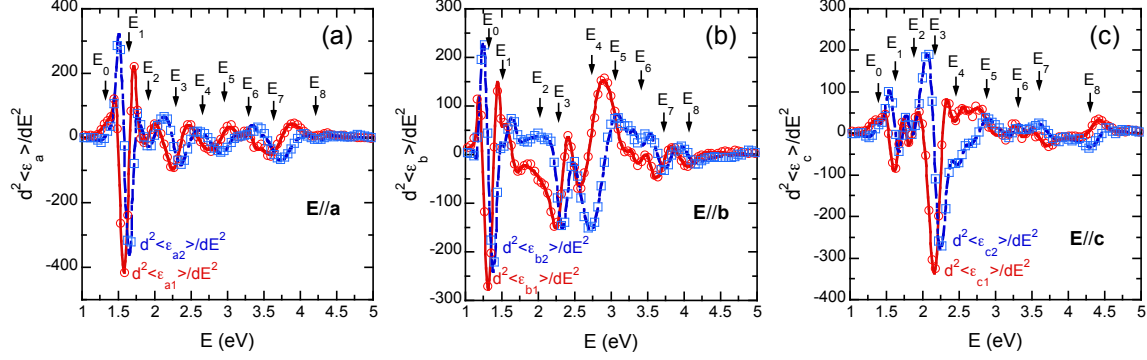


FIG. 5. (Color online) Red solid and blue dash-dotted lines: standard CP lineshapes best fit to second-energy-derivatives $d\langle \epsilon \rangle/dE^2$ (open circles) and $d\langle \epsilon_i \rangle/dE^2$ (open squares) for the light polarization of (a) $\vec{E} \parallel \vec{a}$, (b) $\vec{E} \parallel \vec{b}$, and (c) $\vec{E} \parallel \vec{c}$, respectively. The $d\langle \epsilon \rangle/dE^2$ and $d\langle \epsilon_i \rangle/dE^2$ data are calculated as described in the text. For clarity, only 20% of the data points are shown. Energies of each CP structure are indicated by arrows and labeled in a numeric order.

The calculated and fit-determined CP energies are listed in Table II. The energy values reported in previous studies^{32,48,49,53} are also included for comparison. For the light polarization $\vec{E} \parallel \vec{a}$ and $\vec{E} \parallel \vec{b}$, our data are in a good agreement with the results from previous studies. However, our data reveal two additional CP structures for those two light polarizations, and also provide the CP energies in SnS for the light polarization $\vec{E} \parallel \vec{c}$ that have not yet been obtained experimentally.

Table II. Fit-determined CP energies in eV for α -SnS. Calculated and previously reported CP energies are also included for comparison. Suggested symmetric point in Brillouin zone for each CP structure is listed.

CP	Theory – Symmetric points (k, k, k)	$\vec{E} \parallel \vec{a}$	$\vec{E} \parallel \vec{b}$	$\vec{E} \parallel \vec{c}$
E ₀	1.11 ^{ind.} / 1.22 ^{dir.}	1.36 ^a , 1.3 ^d	1.31 ^a , 1.21 ^b , 1.3 ^c	1.32 ^c
E ₁	1.87 – (0.0,0.0,0.0); Γ	1.59 ^a , 1.54 ^b / 1.6 ^b , 1.6 ^c	1.60 ^b , 1.59 ^d	1.61 ^a , 1.54 ^c
E ₂	1.90 – (0.5,0.0,0.5); U	1.91 ^a	1.98 ^b , 1.91 ^d	1.87 ^c
E ₃	1.97 – (0.0,0.0,0.5); Z	2.28 ^a , 2.23 ^b , 2.36 ^d , 2.2 ^c	2.34 ^a , 2.35 ^d	2.17 ^c
E ₄	2.45 – (0.0,0.5,0.0); Y	2.64 ^a , 2.72 ^b	2.76 ^b , 2.72 ^b , 2.80 ^d	2.43 ^a , 2.44 ^c
E ₅	3.08 – (0.5,0.5,0.0); S	2.98 ^a , 2.82 ^d	3.09 ^a	2.84 ^c
E ₆	3.96 – (0.5,0.0,0.0); X	3.29 ^a , 3.47 ^b , 3.5 ^c	3.42 ^a , 3.41 ^b , 3.56 ^d , 3.3 ^c	3.29 ^c
E ₇	5.23 – (0.5,0.5,0.5); R	3.71 ^b , 3.93 ^b , 3.7 ^d	3.70 ^b , 3.68 ^d	3.64 ^a , 3.99 ^b
E ₈	5.28 – (0.0,0.5,0.5); T	4.30 ^b , 4.41 ^d , 4.3 ^c	4.06 ^c , 4.17 ^b , 4.5 ^c	4.38 ^a , 4.59 ^b

^aThis work – Exp.

^bRef. 48 – Theory.

^cRef. 49 – Exp.

^dRef. 53 – Exp.

^eRef. 32 – Exp.

V. CONCLUSIONS

An experiment and theory combined study has been performed on the anisotropic optical properties of α -phase SnS. Spectroscopic ellipsometry (SE) has been used to determine the pseudo-dielectric-function tensor $\langle \epsilon \rangle = \langle \epsilon_r \rangle + i\langle \epsilon_i \rangle$ spectra of α -SnS single crystal at the light polarizations of $\vec{E} \parallel \vec{a}$, $\vec{E} \parallel \vec{b}$, and $\vec{E} \parallel \vec{c}$. The SE data clearly show a biaxial anisotropy in the optical properties of SnS, which is supported by the results of the calculated dielectric response from hybrid density functional theory (DFT). The calculations also predict that SnS possesses an indirect band gap of 1.11 eV and a direct gap of 1.22 eV for all three crystallographic orientations. Our SE data do not resolve the indirect band gap, but lineshape analysis of the second-energy-derivative of $\langle \epsilon \rangle$ spectra reveals the direct band gap at ~ 1.3 eV. In addition to the direct band-gap onset, a total of eight above-band-gap critical-point (CP) structures were analyzed in the $d\langle \epsilon \rangle / dE^2$ spectra in the spectral range of 1.0 to 5.0 eV. Probable electronic origin of each CP structure observed was identified based on the results from our hybrid DFT calculations. Our SE data establish the optical function spectra of α -SnS in the three crystallographic orientations, which can be used as a reference for optical characterization of polycrystalline SnS thin films. The results from our comparison study of experimental data analysis and DFT calculations improve our understanding of the electronic structure of SnS for better design of SnS-based photovoltaic devices.

ACKNOWLEDGMENTS

This work was supported by the U.S. Department of Energy as a part of the Non-Proprietary Partnering Program at the National Renewable Energy Laboratory under Contract No. DE-AC36-08-GO28308. A.W. acknowledges support from the Royal Society for a University Research Fellowship, and L.A.B. was funded by EPSRC (Grant No. EP/G03768X/1). Calculations were performed with the use of the IRIDIS High Performance Computing Facility, and associated support services at the University of Southampton.

REFERENCES

- ¹A. R. H. F. Ettema, R.A. de Groot, and C. Haas, Phys. Rev. B **46**, 7363 (1992).
- ²M. Devika, N.K. Reddy, K. Ramesh, R. Ganesan, K.R. Gunasekhar, E.S.R. Gopal, and K.T.R. Reddy, J. Electrochem. Soc. **154**, H67 (2007).
- ³R.E. Banai, H. Lee, M.A. Motyka, R. Chandrasekharan, N.J. Podraza, J.R.B. Brownson, and M.W. Horn, IEEE J. Photovoltaics **3**, 1084 (2013).
- ⁴A. Wangperawong, S.M. Herron, R.R. Runser, C. Hägglund, J.T. Tanskanen, H.B.R. Lee, B.M. Clemens, S.F. Bent, Appl. Phys. Lett., 103052105 (2013).
- ⁵J.L. Loferski, J. Appl. Phys. **27**, 777 (1956).
- ⁶K. Hartman, R. Jaramillo, V. Steinmann, R. Chakraborty, H.H. Park, R.G. Gordon, and T. Buonassisi, MRS Fall Meeting (Boston, 2013).
- ⁷M.A. Green, K. Emery, Y. Hishikawa, W. Warta, and E.D. Dunlop, Prog. Photovolt.: Res. Appl. **22**, 1 (2014).
- ⁸P. Sinsermsuksakul, J. Heo, W. Noh, A.S. Hock, and R.G. Gordon, Adv. Energy Mater. **1**, 1116 (2011).
- ⁹L.A. Burton and A. Walsh, Appl. Phys. Lett. **102**, 132111 (2013).
- ¹⁰L.A. Burton, D. Colombara, R.D. Abellon, F.C. Grozema, L.M. Peter, T.J. Savenije, G. Dennler, and A. Walsh, Chem. Mater. **25**, 4908 (2013).
- ¹¹J. Koh, H. Fujiwara, Y. Lu, C.R. Wronski, and R.W. Collins, Thin Solid Films **313-314**, 469 (1998).
- ¹²M.I. Alonso, M. Garriga, C.A. Durante Rincón, E. Hernández, and M. León, Appl. Phys. A **74**, 659 (2002).
- ¹³H. Fujiwara and M. Kondo, Phys. Rev. B **71**, 075109 (2005).
- ¹⁴M.A. Steiner, J.F. Geisz, I. García, D.J. Friedman, A. Duda, and S.R. Kurtz, J. Appl. Phys. **113**, 123109 (2013).
- ¹⁵M. Law, M.C. Beard, S. Choi, J.M. Luther, M.C. Hanna, and A.J. Nozik, Nano Lett. **8**, 3904 (2008).

- ¹⁶S.G. Choi, M. van Schilfgaarde, D.E. Aspnes, A.G. Norman, J.M. Olson, T.J. Peshek, and D.H. Levi, *Phys. Rev. B* **83**, 235210 (2011).
- ¹⁷S.G. Choi, H.Y. Zhao, C. Persson, C.L. Perkins, A.L. Donohue, B. To, A.G. Norman, J. Li, and I.L. Repins, *J. Appl. Phys.* **111**, 033506 (2012).
- ¹⁸S.G. Choi, J. Hu, L.S. Abdallah, M. Limpinsel, Y.N. Zhang, S. Zollner, R.Q. Wu, and M. Law, *Phys. Rev. B* **86**, 115207 (2012).
- ¹⁹S.G. Choi, R. Chen, C. Persson, T.J. Kim, S.Y. Hwang, Y.D. Kim, and L.M. Mansfield, *Appl. Phys. Lett.* **101**, 261903 (2012).
- ²⁰Z. Zainal, M.Z. Hussein, and A. Ghazali, *Sol. Energy Mater. Sol. Cells* **40**, 347 (1996).
- ²¹S. Lopez and A. Ortiz, *Semicond. Sci. Technol.* **9**, 2130 (1994).
- ²²Yanuar, F. Guastavino, C. Llinares, K. Djessas, and G. Masse, *J. Mater. Sci. Lett.* **19**, 2135 (2000).
- ²³M. Calixto-Rodriguez, H. Martinez, A. Sanchez-Juarez, J. Campos-Alvarez, A. Tiburcio-Silver, and M. Calixto, *Thin Solid Films* **517**, 2497 (2009).
- ²⁴N.K. Reddy and K.T.R. Reddy, *Mater. Chem. Phys.* **102**, 13 (2007).
- ²⁵B. Ghosh, M. Das, P. Banerjee, and S. Das, *Appl. Surf. Sci.* **254**, 6436 (2008).
- ²⁶O.E. Ogah, G. Zoppi, I. Forbes, and R. Miles, *Thin Solid Films* **517**, 2485 (2009).
- ²⁷T.H. Sajeesh, N. Poornima, C. Sudha Kartha, and K.P. Vijayakumar, *Phys. Status Solidi a* **207**, 1934 (2010).
- ²⁸J. Vidal, S. Lany, M. d’Avezac, A. Zunger, A. Zakutayev, J. Francis, and J. Tate, *Appl. Phys. Lett.* **100**, 032104 (2012).
- ²⁹L.L. Cheng, M.H. Liu, M.X. Wang, S.C. Wang, G.D. Wang, Q.Y. Zhou, and Z.Q. Chen, *J. Alloys and Compounds* **545**, 122 (2012).
- ³⁰E.R. Shaaban, M.S. Abd El-Sadek, M. El-Hagary, and I.S. Yahia, *Phys. Scr.* **86**, 015702 (2012).
- ³¹H.R. Chandrasekhar, R.G. Humphreys, U. Zwick, and M. Cardona, *Phys. Rev. B* **15**, 2177 (1977).
- ³²R. Eymard and A. Otto, *Phys. Rev. B* **16**, 1616 (1977).
- ³³A.P. Lambros, D. Geraleas, and N.A. Economou, *J. Phys. Chem. Solids* **35**, 537 (1974).

- ³⁴L. Viña, S. Logothetidis, and M. Cardona, Phys. Rev. B **30**, 1979 (1984).
- ³⁵S. Zollner, M. Garriga, J. Humlíček, S. Gopalan, and M. Cardona, Phys. Rev. B **43**, 4349 (1991).
- ³⁶T. Sorgenfrei, F. Hofherr, T. Jauß, and A. Cröll, Cryst. Res. Technol. **48**, 193 (2013).
- ³⁷D.E. Aspnes, J. Opt. Soc. Am. **70**, 1275 (1980).
- ³⁸G.E. Jellison, Jr. and J.S. Baba, J. Opt. Soc. Am. A **23**, 468 (2006).
- ³⁹J. Heyd, G. E. Scuseria, and M. Ernzerhof, J. Chem. Phys. **124**, 219906 (2006).
- ⁴⁰G. Kresse and J. Furthmüller, Phys. Rev. B **54**, 11169 (1996).
- ⁴¹G. Kresse and D. Joubert, Phys. Rev. B **59**, 1758 (1999).
- ⁴²T. Chattopadhyay, J. Pannetier, and H.G. Von Schnering J. Phys. Chem. Solids **47**, 879 (1986).
- ⁴³M. Gajdos, K. Hummer, G. Kresse, J. Furthmüller, and F. Bechstedt, Phys. Rev. B **73**, 045112 (2006).
- ⁴⁴M. Parenteau and C. Carlone, Phys. Rev. B **41**, 5227 (1990).
- ⁴⁵W. Albers, C. Haas, H. J. Vink, and J.D. Wasscher, J. Appl. Phys. **32**, 2220 (1961).
- ⁴⁶O. Madelung, Semiconductors: Data Handbook, 3rd ed. (Springer, New York, 2004), p. 578.
- ⁴⁷D.E. Aspnes, in *Handbook of Optical Constants of Solids*, edited by E.D. Palik (Academic, Orlando, 1985), Vol. I, p.89.
- ⁴⁸L. Makinistian and E.A. Albanesi, Phys. Status Solidi b **246**, 183 (2009).
- ⁴⁹G. Valiukonis, D.A. Guseinova, G. Krivaitė, and A. Sileika, Phys. Status Solidi b **135**, 299 (1986).
- ⁵⁰A. Savitzky, and M.J.E. Golay, Anal. Chem. **36**, 1627 (1964).
- ⁵¹M. Cardona, *Modulation Spectroscopy, Suppl. 11 of Solid State Physics* (Academic, New York, 1969), p 119.
- ⁵²D.E. Aspnes, in *Handbook of Semiconductors*, edited by M. Balkanski (North-Holland, Amsterdam, 1980), Vol. 2, p. 109.
- ⁵³F. Lukes, J. Humlíček, and E. Schmidt, Solid State Commun. **45**, 445 (1983).